3. Tang, C. W., VanSlyke, S. A. & Chen, C. H. Electroluminescence of doped organic thin films. *J. Appl. Phys.* **65,** 3610–3616 (1989).
4. Tsutsui, T. & Saito, S. *Organic Multilayer-Dye Electroluminescent Diodes—Is There Any Difference with Polymer LED?* (Kluwer Academic, Dordrecht, 1993).
5. Rothberg, L. J. & Lovinger, A. J. Status of and prospects for organic electroluminescence. *J. Mater. Res.* **11,** 3174–3187 (1996).
6. Gu, G. *et al.* High-external-quantum-efficiency organic light-emitting devices. *Opt. Lett.* **22,** 396–398 (1997).
7. Dirr, S. *et al.* Vacuum-deposited thin films of lanthanide complexes: spectral properties and applications in organic light-emitting devices. In *SID 97 Digest* (ed. Morreale, J.) 778–781 (Soc. for Information Display, Santa Ana, CA, 1997).
8. Hoshino, S. & Suzuki, H. Electroluminescence from triplet excited states of benzophenone. *Appl. Phys. Lett.* **69,** 224–226 (1996).
9. Mills, A. & Lepre, A. Controlling the response characteristics of luminescent porphyrin plastic film sensors for oxygen. *Anal. Chem.* **69,** 4653–4659 (1997).
10. Ponterini, G., Serpone, N., Bergkamp, M. A. & Netzel, T. L. Comparison of radiationless decay processes in osmium and platinum porphyrins. *J. Am. Chem. Soc.* **105,** 4639–4645 (1983).
11. Papkovski, D. B. New oxygen sensors and their applications to biosensing. *Sens. Actuators B* **29,** 213–218 (1995).
12. Turro, N. J. *Modern Molecular Photochemistry* (University Science Books, Mill Valley, CA, 1991).
13. Liu, H.-Y., Switalski, S. C., Coltrain, B. K. & Merkel, P. B. Oxygen permeability of sol-gel coatings. *Appl. Spectrosc.* **46,** 1266–1272 (1992).
14. Rodriguez, J., McDowell, L. & Holten, D. Elucidation of the role of metal to ring charge-transfer states in the deactivation of photo-excited ruthenium porphyrin carbonyl complexes. *Chem. Phys. Lett.* **147,** 235–240 (1988).
15. Bulovic, V. *et al.* Bright, saturated, red-to-yellow organic light-emitting devices based on polarization-induced spectral shifts. *Chem. Phys. Lett.* **287,** 455–460 (1998).
16. Chen, C. H., Tang, C. W., Shi, J. & Klubeck, K. P. Improved red dopants for organic electroluminescent devices. *Macromol. Symp.* **125,** 49–58 (1997).
17. Tsutsui, T., Takada, N., Saito, S. & Ogino, E. Sharply directed emission in organic electroluminescent diodes with an optical-microcavity structure. *Appl. Phys. Lett.* **65,** 1868–1870 (1994).
18. Kido, J. *et al.* Bright red light emitting organic electroluminescent devices having a europium complex as an emitter. *Appl. Phys. Lett.* **65,** 2124–2126 (1994).
19. Sano, T. *et al.* Novel europium complexes for electroluminescent devices with sharp red emission. *Jpn J. Appl. Phys.* **34,** 1883–1887 (1994).
20. Garbuzov, D. Z., Bulovic, V., Burrows, P. E. & Forrest, S. R. Photoluminescence efficiency and absorption of aluminum-tris-quinolate (Alq_3) thin films. *Chem. Phys. Lett.* **249,** 433–437 (1996).

Acknowledgements. We thank V. G. Kozlov for help with the transient measurements, and P. E. Burrows for discussions. This work was supported by Universal Display Corporation, DARPA, AFPSR and NSF.

Correspondence and requests for materials should be addressed to S.R.F. (forrest@ee.princeton.edu).

Synthesis and organization of zeolite-like materials with three-dimensional helical pores

Thurman E. Gier, Xianhui Bu, Pingyun Feng & Galen D. Stucky

Department of Chemistry, University of California, Santa Barbara, California 93106, USA

The increasing demand for enantiomerically pure chemicals has stimulated extensive research into the preparation of heterogeneous chiral catalysts or separation media that combine both shape selectivity and enantioselectivity[1]. Helical pores in inorganic materials might be able to perform such functions, but their occurrence is rare[1]. Attempts have been reported to synthesize a specific enantiomorph of the chiral zeolite beta[2], and chiral metal complexes have been used to assemble inorganic precursors into chiral frameworks[3,4]. Materials with a fully three-dimensional array of helical structural units are particularly rare, because helical structures (such as quartz) are commonly generated by a uni-dimensional symmetry element acting on an achiral structural subunit[5,6]. Here we report on a family of zeolite-type materials (which we call UCSB-7) that possess two independent sets of three-dimensional crosslinked helical pores, separated by a gyroid periodic minimal surface[13]. We have synthesized the UCSB-7 framework for various compositions (zinc and beryllium arsenates, gallium germanate) using either inorganic cations or amines as structure-directing agents. The helical-ribbon motif that we identify might be exploited more widely for developing useful chiral solid-state structures.

The framework topology of UCSB-7 was determined from gallogermanates synthesized with K^+ or amines such as $NH_2(CH_2)_nNH_2$ ($n = 2$–5). We have grown large crystals of gallogermanate phases with a variety of linear and branched mono-, di- or tri-amines

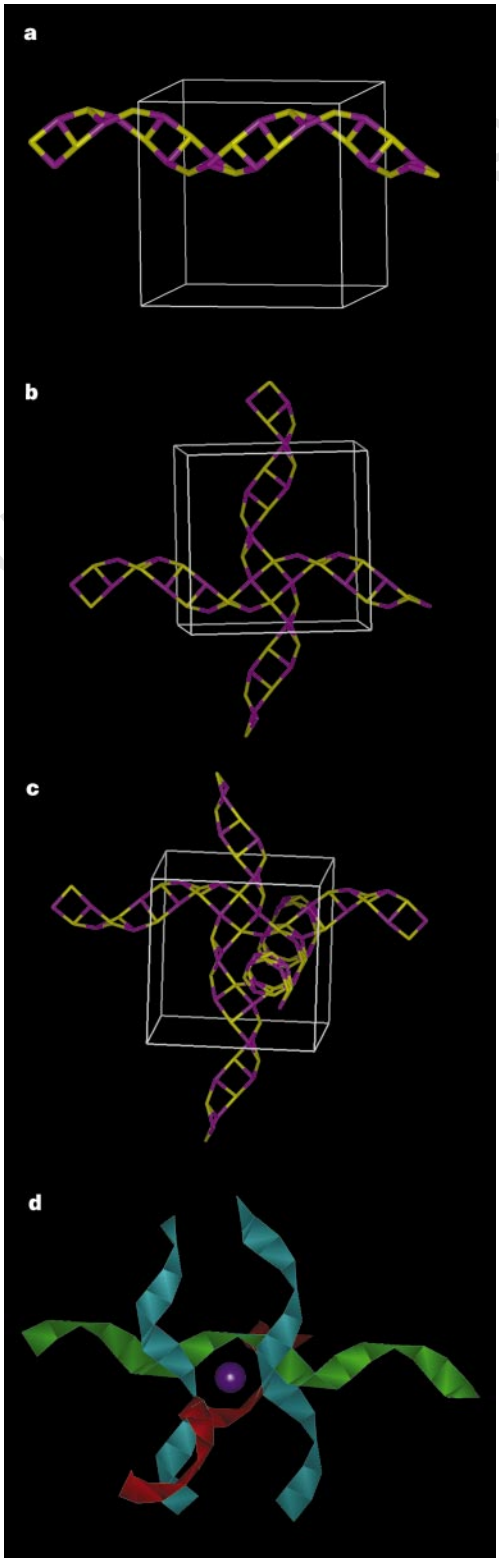

Figure 1 The helical ribbons are crosslinked in three dimensions to give 12-ring pores. From one to three dimensions (**a**–**c**): crosslinking of mutually perpendicular inorganic helical chains in UCSB-7K. In all panels the bridging oxygen atoms are omitted. The yellow sites represent Ge^{4+} atoms and the purple sites Ga^{3+} atoms. **d**, The K^+ ion channel with the 12-ring pore. The purple sphere represents the K^+ ion.

including methylamine, *N*-methylethylenediamine, tris(2-aminoethylamine), *N*-(2-aminoethyl)-1,3-propanediamine and 3,3′-diamino-*N*-methyldipropylamine. An exceptional case is the successful use of poly(ethylenimine), an organic polymer, in the synthesis of UCSB-7. We identified non-gallogermanate phases on the basis of powder diffraction patterns, all of which can be indexed by using a body-centred cubic cell with a repeat distance of ~18 Å. Another zeolite structure with the 18-Å body-centred cubic cell is ZK-5, but it has very different lattice symmetry ($Im\bar{3}m$), leading to a different powder diffraction pattern.

Of particular interest is the synthesis of the ethylenediamine zinc arsenate phase UCSB-7 at freezing temperatures (from −20 to 4 °C). At 25 °C, it transforms into UCSB-3 within a few days and at 100 °C, UCSB-3 is formed within 20 min (ref. 7). The ethylenediamine gallogermanate phase is, however, much more stable and its crystals have been grown at 180 °C, together with UCSB-3GaGe and GaGe-SOD1 (a triclinic sodalite analogue). The framework structure of UCSB-7 is not stable to water loss in the range 250–400 °C depending on the chemical composition. However, essentially complete replacement of K^+ by NH_4^+ in saturated NH_4HCO_3 solution at 10 °C was easily accomplished and established by the recovery of clean $Ga_2Ge_2O_7$ after pyrolysis at 1,000 °C. The Ge/Ga ratio in gallogermanates can be manipulated by using different structure-directing agents. For example, in UCSB-7dma (here, dma is dimethylamine), the Ge/Ga ratio is 3 on the basis of crystal structure analysis and electron-probe elemental analysis.

UCSB-7 consists of two helical–T–O–T–atomic chains (T refers to tetrahedral atoms) with the same handedness that are coupled together to form a helical ribbon made up of edge-sharing 4-rings (Fig. 1). The pitch of the helix is equal to the unit cell repeat length and the width is ~5.7 Å for gallogermanate phases based on the distance between T-atoms. Each helical turn contains eight 4-rings (Fig. 1). The cylindrical volume within each helical ribbon forms a channel along a unit cell axis, and, when projected along the axis, the channel seems to have an 8-ring aperture (see Fig. 2a). In fact there is no closed 8-ring anywhere in the structure: only 4-, 6- and 12-rings are present. There are too few atoms on the helical ribbons to completely isolate the channel spaces along the axes of the helices. However, the connectivity of the helical ribbons (see Figs 1 and 3) orientated along the three cubic axes does give rise to 12-ring windows and the pore structure (see Figs 2 and 3). When viewed down the cubic unit cell body-diagonal directions, the disposition of these 12-ring channels is easily seen (Fig. 2b).

The interconnection by 12-ring windows (Fig. 3a) between the

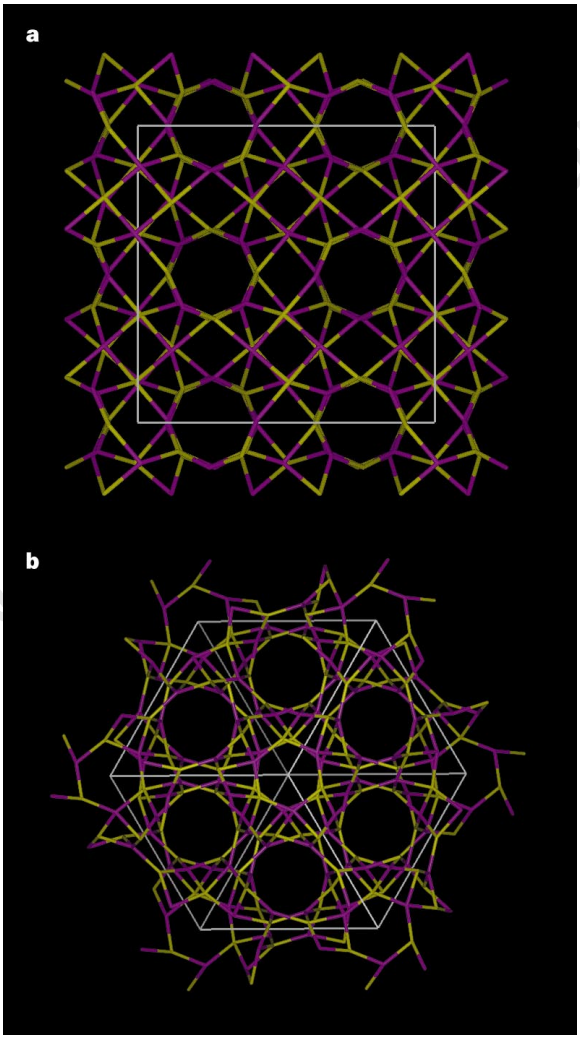

Figure 2 Helices viewed parallel to cubic unit cell edges and body diagonal directions. **a**, The framework structure of UCSB-7K viewed down the *a* axis showing channels that look like 8-ring pores in projection. The apparent walls between channels are in fact other channels that are perpendicular to channels shown here. **b**, The framework structure of UCSB-7K viewed down the crystallographic [111] direction.

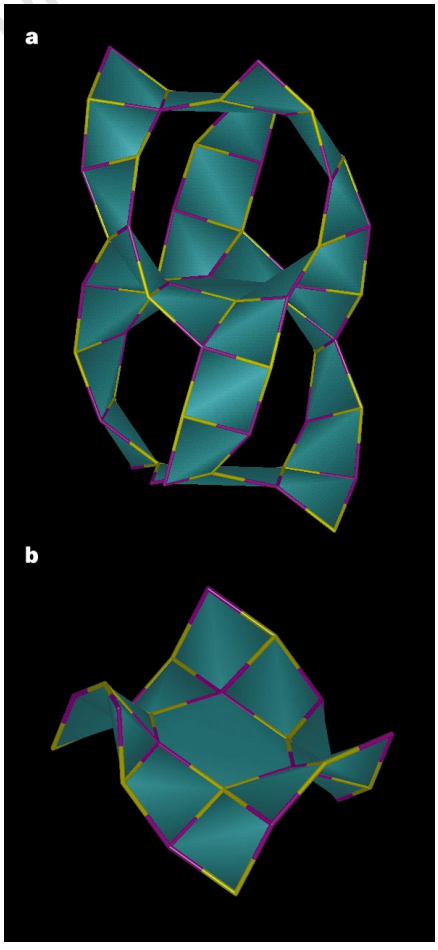

Figure 3 The crystalline gyroid minimal surface of UCSB-7 separates the space into two disconnected volumes. **a**, Two sets of 12-ring windows (three above and three below) are shown here. They connect helices of opposite handedness into two equal but separate volumes. In the middle, a monkey saddle detailed in **b** separates the top portion from the lower one. **b**, A section of the framework surface that can be described as the monkey saddle typical of a gyroid minimal surface. The flat point coincides with the centre of the 6-ring.

void space within helical ribbons occurs only between helices of the same handedness. Every other helical ribbon in Fig. 2a viewed parallel to the cell edge is of opposite handedness, and in general for the structure there are an equal number of right-handed and left-handed helices. Thus, for each helical ribbon, there are four surrounding helical ribbons of the opposite handedness (a/2 Å between channel centres; a is the cell length) and four others of the same handedness ($a\sqrt{2}$/2 Å between channel centres) that are propagating along the same crystallographic direction (Fig. 2a). The interconnections between helices of the same handedness form two equal and disconnected volumes, which in zeolite terms are two independent sets of three-dimensional 12-ring intersecting channels with opposing handednesses. Such a structural feature has not previously been observed in a zeolite-type structure[8]. In fact, even materials with one set of three-dimensional 12-ring channels are rare among known zeolite structures, with zeolite beta, faujasite, hexagonal faujasite (EMC-2), UCSB-6 and UCSB-10 being the only examples[9,10].

The wall that separates the right-handed and left-handed regions can be described as a gyroid bicontinuous minimal surface that has also been found in liquid crystal phases and mesoporous MCM-48[11], except in this case the wall structure is crystalline and well defined at the atomic level. Illustrated in Fig. 3b is a portion of the UCSB-7 wall structure representing a monkey saddle, which is a typical feature of a gyroid surface[12]. For UCSB-7, flat points of such a minimal surface coincide with centres of all 6-rings located at unit cell origins, body-, face- and edge-centres, and on body-diagonals one quarter distance ($a\sqrt{3}$/4 Å) from cell origins. Another zeolite-type structure that has been described by a gyroid surface is a relatively dense phase, analcime[13].

Because both right- and left-handed helices are present, the crystal space group symmetry would be centric $Ia\bar{3}d$ if the tetrahedral framework atoms were all the same or disordered. However, in the case of UCSB-7K, the best results were obtained with an alternative distribution of Ga and Ge sites when the refinement was performed in a non-centric, chiral space group $I2_13$. This was confirmed by the observed difference in metal–oxygen bond distances, which are 1.838 Å for Ga–O and 1.762 Å for Ge–O, in close agreement with those in a gallium germanate sodalite analogue that has bond distances of 1.839 Å for Ga–O and 1.745 Å for Ge–O[14]. With this ordering, the right- and left-handed helices are not mirror images and thus the overall chiral symmetry of UCSB-7 structures is related to framework chemical compositions and ordering of T-atom sites. For example, in UCSB-7 the magnitude of the chirality is determined by the difference in the electrostatic potential at the gallium (negative) and germanium (neutral) atom framework sites, whereas in the zinc or beryllium arsenate structures the chirality would be related to the difference in the electrostatic potentials associated with the zinc or beryllium (negative) and the arsenic (positive) atom framework sites.

We suggest that the formation of the helical pattern is related to the presence of some geometrical features observed in UCSB-7 structures. UCSB-7K has a relatively small T–O–T angle (minimum, maximum and average are 122.3°, 127.0° and 124.2° respectively), consistent with the T–O–T angle found in the gallium germanate sodalite analogue (125.5°) and the T–O–T angles in two arsenate sodalite structures, $Na_3(ZnAsO_4)_3{\cdot}4H_2O$ and $Li_4Cl(BeAsO_4)_3$ of 123.8° and 123.4°, respectively[14,15]. Structurally the small T–O–T angles can be accommodated in a 4-ring that has a UDUD (where U is up and D is down) configuration of the T atoms and therefore the building-block surface curvature and geometry required to generate the helical configuration.

Although a significant amount of the current research on zeolite synthesis is directed at low-charge framework structures, UCSB-7 suggests that there is still a great potential for generating novel zeolite-type structures in the framework charge domain represented by traditional aluminium-rich zeolites[16]. □

Methods

$(KGaGeO_4)_6{\cdot}7H_2O$ (UCSB-7K). To a polypropylene bottle were added 9.26 g 2 M K_5GaO_4 (12 mmol), 15 ml H_2O and 17.47 g 1 M K_6GeO_5 (13 mmol). To the resulting clear solution was added 10.26 g of concentrated HNO_3 (114 mmol), producing a slowly developing gel slurry. After 1 day at 100 °C, the well-settled crystalline powder was filtered off, washed and recovered (2.61 g, 82% yield). The powder diffraction pattern could be indexed by using a body-centred cubic cell. Crystals suitable for single crystal X-ray diffraction were grown by holding the gel slurry at 100 °C for three months (the crystal growth of amine-directed phases usually takes one week at 180 °C). Thermogravimetric analysis to 600 °C gave 8.0% weight loss (calc. = 7.9%). Crystallographic data for $(KGaGeO_4)_6{\cdot}7H_2O$ are: space group $I2_13$; $a = 18.6766(1)$ Å; $V = 6514.69(6)$ Å^3, $Z = 8$, MoKα, $2\theta_{max} = 50°$, $R(F) = 3.82\%$ for 103 parameters and 1,920 reflections with $I > 2\sigma(I)$.

$(NaGaGeO_4)_6{\cdot}xH_2O$ ($x \approx 7$) (UCSB-7Na). To a polypropylene bottle was added 8.80 g 2 M Na_5GaO_4 (12 mmol), 16.04 g 1 M Na_4GeO_4 (13 mmol) and 15 ml H_2O. To the clear solution was then added 8.91 g concentrated HNO_3 (99 mmol), giving a thick milky precipitate. After 7 h at 100 °C, the precipitate was well settled and was recovered (2.945 g, 98% yield). The powder diffraction pattern could be indexed by using a body-centred cubic cell ($a = 18.608$ Å). Thermogravimetric analysis showed 9.3% weight loss (calc. 8.4%), leaving only $NaGaGeO_4$ at 950 °C.

$(NaBeAsO_4)_6{\cdot}xH_2O$ ($x \approx 7$, UCSB-7Be). 4.68 g $Na_2HAsO_4{\cdot}7H_2O$ (15 mmol), 2.142 g 4 M NaOH (7.46 mmol) and 10 ml H_2O were added to a polypropylene bottle to give a clear basic solution; 6.98 g 2 M $Be(NO_3)_2$ (12 mmol) were then added to give a gel slurry with a pH of ~6. After being left for ~20 h at 100 °C, the slurry was well settled and the pH had dropped to 4. Standard filtration and washing techniques yielded 2.17 g (91% yield) of a white powder whose diffraction pattern could be indexed by using a body-centred cubic cell ($a = 17.272$ Å). Thermogravimetric analysis showed 11.0% weight loss to 800 °C (calc. 10.9%).

$(KZnAsO_4)_6{\cdot}xH_2O$ ($x \approx 7$, UCSB-7Zn). 18.60 g 4.8 M H_3AsO_4 (62.75 mmol), 31.03 g 2 M $Zn(NO_3)_2$ (48 mmol) and 20 ml H_2O were added to a polypropylene bottle and then 38.04 g of 5 M KOH was added to the clear solution. The thick gel slurry produced had a pH of ~8. After being left overnight at 25 °C (UCSB-7Zn can also be made at 4 °C, but is unstable at 100 °C), the slurry was well settled and on filtration and washing yielded 11.8 g (91% yield) of a white microcrystalline powder whose diffraction pattern could be indexed by using a body-centred cubic cell ($a = 18.710$ Å). Thermogravimetric analysis showed a 9.5% weight loss to 450 °C (calc. = 7.9% for $x = 7$) occurring in two steps. The residue was determined as being monoclinic $KZnAsO_4$ by X-ray diffraction. Use of the same procedure, but with up to 20% of the zinc replaced by Co^{2+}, Mn^{2+} or Fe^{2+}, resulted in clean single-phase products (blue, faint pink and green–grey, respectively), indicating the possible replacement of zinc sites by transition metals. The maximum possible substitution levels have not been determined.

$(EDA)_3(ZnAsO_4)_6{\cdot}xH_2O$ (UCSB-7EDA). 2.40 g ethylenediamine (40 mmol), 10 ml H_2O and 7.71 g 2 M $Zn(NO_3)_2$ (12 mmol) were added to a small polypropylene bottle. The initial precipitate redissolved and the clear solution was then cooled to ~4 °C in a refrigerator. After the solution had chilled, 4.74 g 4 M H_3AsO_4 (14 mmol) was added and the resulting gel slurry was returned to the refrigerator (pH 8.5). After 2 days at 4 °C, the gel was well crystallized and recovery yielded 1.15 g (33% yield) of material whose powder pattern was indexed by using a body-centred cubic cell ($a = 18.957$ Å). UCSB-7EDA can also be made at −20 °C at a slower crystallization speed.

Received 27 April; accepted 13 July 1998.

1. Baiker, A. Chiral catalysis on solids. *Curr. Opin. Solid State Mater. Sci.* **3,** 86–93 (1998).
2. Davis, M. E. New vistas in zeolite and molecular sieve catalysis. *Acc. Chem. Res.* **26,** 111–115 (1993).
3. Bruce, D. A., Wilkinson, A. P., White, M. G. & Bertrand, J. A. The synthesis and characterization of an aluminophosphate with chiral layers: trans-$Co(dien)_2{\cdot}Al_3P_4O_{16}{\cdot}3H_2O$. *J. Solid State Chem.* **125,** 228–233 (1996).
4. Morgan, K., Gainsofrd, G. & Milestone, N. A novel layered aluminum phosphate [Co(en) $Al_3P_4O_{16}{\cdot}3H_2O$] assembled about a chiral metal complex. *J. Chem. Soc. Chem. Commun.* 425–426 (1995).
5. Harrison, W. T. A., Gier, T. E., Stucky, G. D., Broach, R. W. & Bedard, R. A. $NaZnPO_4{\cdot}H_2O$, an open-framework sodium zincophosphate with a new chiral tetrahedral framework topology. *Chem. Mater.* **8,** 145–151 (1996).
6. Soghomonian, V., Chen, Q., Haushalter, R. C., Zubieta, J. & O'Connor, C. J. An inorganic double helix: hydrothermal synthesis, structure, and magnetism of chiral $[(CH_3)_2NH_2]K_4[V_{10}O_{10}(H_2O)_2(OH)_4(PO_4)_7]{\cdot}4H_2O$. *Science* **259,** 1596–1599 (1993).

7. Bu, X., Feng, P., Gier, T. E. & Stucky, G. D. Two ethylenediamine templated zeolite type structure sin zinc arsenate and cobalt phosphate systems. *J. Solid State Chem.* **136,** 210–215 (1998).
8. Smith, J. V. Topochemistry of zeolites and related materials. 1. Topology and geometry. *Chem. Rev.* **88,** 148–182 (1988).
9. Meier, W. M., Olson, D. H. & Baerlocher, C. *Atlas of Zeolite Structure Types* (Elsevier, Boston, 1996).
10. Bu, X., Feng, P. & Stucky, G. D. Large-cage zeolite structures with multidimensional 12-ring channels. *Science* **278,** 2080–2085 (1997).
11. Monnier, A. *et al.* Cooperative formation of inorganic–organic interfaces in the synthesis of silicate mesostructures. *Science* **261,** 1299–1303 (1994).
12. Andersson, S. & Jacob, M. *The Mathematics of Structures* (R. Oldenbourg, München, 1997).
13. Andersson, S., Hyde, S. T., Larsson, K. & Lidin, S. Minimal surfaces and structures: from inorganic and metal crystals to cell membranes and biopolymers. *Chem. Rev.* **88,** 221–242 (1988).
14. Nenoff, T. M. *et al.* Structural and chemical investigations of $Na_3(ABO_4)_3{\cdot}4H_2O$-type sodalite phases. *Inorg. Chem.* **33,** 2472–2480 (1994).
15. Harrison, W. T. A., Gier, T. E. & Stucky, G. D. Two lithium chloroberyllo(phosphate/arsenate) sodalites: $Li_4Cl(BePO_4)_3$ and $Li_4Cl(BeAsO_4)_3$. *Acta Crystallogr. C* **50,** 471–473 (1994).
16. Feng, P., Bu, X. & Stucky, G. D. Hydrothermal synthesis and structural characterization of zeolite analogue compounds based on cobalt phosphate. *Nature* **388,** 735–741 (1997).

Supplementary Information is available on *Nature*'s World-Wide Web site (http://www.nature.com) or as paper copy from the London editorial office of *Nature*.

Acknowledgements. This research was supported in part by the National Science Foundation and the Office of Naval Research. P.F. thanks the Materials Research Laboratory for a Corning Foundation Fellowship. All figures were generated using software programs from Molecular Simulations.

Correspondence and requests for materials should be addressed to G.D.S. (e-mail: stucky@chem.ucsb.edu).

Heterogeneous production of nitrous acid on soot in polluted air masses

M. Ammann*, M. Kalberer*†, D. T. Jost*, L. Tobler*, E. Rössler*, D. Piguet*, H. W. Gäggeler*† & U. Baltensperger*

** Paul Scherrer Institute, Laboratory of Radio- and Environmental Chemistry, CH-5232 Villigen, Switzerland*

† University of Bern, Department of Chemistry and Biochemistry, CH-3012 Bern, Switzerland

Polluted air masses are characterized by high concentrations of oxidized nitrogen compounds which are involved in photochemical smog and ozone formation. The OH radical is a key species in these oxidation processes. The photolysis of nitrous acid (HNO_2), in the morning, leads to the direct formation of the OH radical and may therefore contribute significantly to the initiation of the daytime photochemistry in the polluted planetary boundary layer. But the formation of nitrous acid remains poorly understood: experimental studies imply that a suggested heterogeneous formation process involving NO_2 is not efficient enough to explain the observed night-time build-up of HNO_2 in polluted air masses[1]. Here we describe kinetic investigations which indicate that the heterogeneous production of HNO_2 from NO_2 on suspended soot particles proceeds 10^5 to 10^7 times faster than on previously studied surfaces. We therefore propose that the interaction between NO_2 and soot particles may account for the high concentrations of HNO_2 in air masses where combustion sources contribute to air pollution by soot and NO_x emissions. We believe that the observed HNO_2 formation results from the reduction of NO_2 in the presence of water by C–O and C–H groups in the soot. Although prolonged exposure to oxidizing agents in the atmosphere is likely to affect the chemical activity of these groups, our observations nevertheless suggest that fresh soot may have a considerable effect on the chemical reactions occurring in polluted air.

There is strong evidence that the spatial and temporal distribution of HNO_2 throughout the planetary boundary layer (PBL) is governed by continuous formation and daytime photolysis, which result in pronounced diurnal cycles with night-time maxima of up to more than 10 parts per billion by volume (p.p.b.v.). Correlation analysis points to NO_2 as a source component, and typical NO_2 conversion rates inferred are $10^{-6}\,s^{-1}$ (refs 2–4). The gas phase reaction of OH radicals with NO may only contribute significantly to the very low HNO_2 levels found during the day. HNO_2 emitted directly from combustion processes, together with other oxidized nitrogen compounds and soot, is of minor importance[5]. Therefore, a heterogeneous process involving NO_2 has been suggested. The maximum surface area per unit volume, S/V, attributed to ground and airborne surfaces is $10^{-2}\,cm^{-1}$ and $10^{-5}\,cm^{-1}$, respectively, for typical mixing heights (minimum, 100 m during the night) in the PBL. These surfaces have been proposed to catalyse the reaction between NO_2 and H_2O to form nitric and nitrous acid (reaction (1)), but measured HNO_2 formation rates using different types of bulk surfaces (solid materials and aqueous solutions) were found to be two to five orders of magnitude smaller than the NO_2 to HNO_2 conversion rates inferred from atmospheric observations[1].

$$2NO_2 + H_2O = HNO_3 + HNO_2 \quad (1)$$

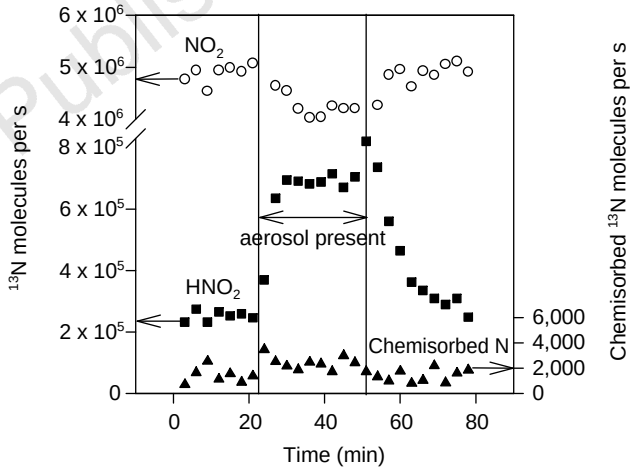

Figure 1 Online record of the rate of $H^{13}NO_2$ formation from 12 p.p.b.v. NO_2 in the absence and presence of soot particles. The data, obtained over a period of 80 min, record the rate of $H^{13}NO_2$ formation 20 s after two different gas flows have been mixed in a flow reactor at 22 °C, ambient pressure and 50% relative humidity. The first gas flow, containing NO_2 (enriched with $^{13}NO_2$) in He and 20% O_2, is introduced at a rate of $5\,cm^3\,s^{-1}$. The $^{13}NO_2$ content is adjusted so that the $^{13}NO_2$ molecules are fed into the reactor at a rate of $5 \times 10^6\,s^{-1}$. The NO_x-free soot aerosol is produced with a pulsed spark discharge between graphite rods in Ar, followed by dilution with air and a thermodenuder operating at 400 °C. O_2, N_2 and H_2O impurities in the Ar (99.998%) give rise to soot-like complex organic carbon compounds on the particle surfaces. Before introducing the gas mixture containing the aerosol into the reactor at a rate of $13.3\,cm^3\,s^{-1}$, part of the flow is passed through a differential mobility analyser coupled to a condensation particle counter to monitor the concentration and size distribution of the aerosol. The total flow rate through the 80-cm-long glass reactor (2.5 cm inner diameter) is $18.3\,cm^3\,s^{-1}$, and the gas mixture contains 14% O_2, 47% N_2, 13% He, 26% Ar, 1.2% H_2O and 12 p.p.b.v. NO_2. For product detection and identification, 5 compound-specific 40-cm-long glass denuders (4 mm inner diameter) were designed as coils around the γ-ray detectors (5.5 cm diameter). The first was coated with sodium chloride (HNO_3 detection), the second and third with a sodium carbonate/glycerol mixture (HNO_2), the fourth with a triethanolamine/guaiacol mixture (NO_2), and the fifth with cobalt(II/III) oxide (NO). For HNO_2, the two denuders with the same coating in series allowed a correction for interference by NO_2. The γ-ray activities measured at the denuders (NO_2 and HNO_2) and at the filter (N_{chem}) were converted to fluxes of molecules into each trap using the 9.96-min half-life of ^{13}N. In each experiment, the background effect caused by the reaction of NO_2 to HNO_2 at the glass walls of the flow reactor (reaction (1)) was measured before and after the soot particles were present.